Vol. 92 No. 1 pp. 342–353 ACTA GEOLOGICA SINICA (English Edition) Feb. 2018

Pore Types and Quantitative Evaluation of Pore Volumes in the Longmaxi Formation Shale of Southeast Chongqing, China

CHEN Fangwen*, LU Shuangfang and DING Xue

Research Institute of Unconventional Oil & Gas and Renewable Energy, China University of Petroleum (East China), Qingdao 266580, Shandong, China

Abstract: The common microscale to nanoscale pore types were introduced and divided into organic and inorganic pores to estimate their contributions to porosity in the Lower Silurian Longmaxi Formation shale of southeast Chongqing. Following the material balance principle, the organic porosity values, which changed with formation subsidence and thermal evolution, were calculated using chemical kinetics methods and corrected via the organic porosity correction coefficient, which was obtained from field emission scanning electron microscopy. Grain density values were determined using the contents and true densities of compositions in the shale samples. The total porosity was calculated based on the grain and bulk densities. The inorganic porosity was determined from the difference between the total porosity and organic porosity at the same depth. The results show that inorganic pores mainly contain microfractures, microchannels, clay intergranular pores, intercrystalline pores and intracrystalline pores in the Lower Silurian Longmaxi Formation shale of southeast Chongqing. Organic pores mainly include organopore and fossil pore. The total porosity, organic porosity and inorganic porosity of organic-rich shale samples can be quantitatively evaluated using this method. The total porosity, organic porosity and inorganic porosity values of the Longmaxi Formation shale samples from the well Py1 in southeast Chongqing lie in 2.75%–6.14%, 0.08%–2.52% and 1.41%–4.92% with average values of 4.34%, 0.95% and 3.39%, respectively. The contributions of the inorganic pores to the total porosity are significantly greater than those of the organic pores.

Key words: southeast Chongqing, Longmaxi Formation shale, total porosity, organic porosity, inorganic porosity

1 Introduction

Microscale and nanoscale pores, total organic carbon (TOC) and maturity of a shale reservoir play key roles in the accumulation of shale gas. Nanoscale pores in a shale reservoir are mainly organopores (pores within shale that contain organic matter) created via hydrocarbon generation (Loucks et al., 2009; Liu Shugen et al., 2011; Chalmers et al., 2012; Xiao Xianming et al., 2015; Zhao Wenzhi et al., 2016; Zhao Jianhua et al., 2016; Wei Xiangfeng et al., 2017). Numerous scholars have studied organic pores in shale reservoirs and believe that organopores form in organic matter as a result of hydrocarbon generation and contribute significantly to volume of pores (Jarvie et al., 2007; Curtis et al., 2010; Christopher et al., 2012; Han Shuangbiao et al., 2013; Chen Lei et al., 2017). In addition, the specific surface area of organopores heavily affects the amount of the adsorbed shale gas (Ambrose et al., 2010; Curtis et al., 2012; Mosher et al., 2013; Chen et al., 2017). Conventional methods such as mercury intrusion porosimetry and nuclear magnetic resonance cannot effectively measure organopores in shale reservoir, which are a few to tens of nanometres in width (Howard, 1991). Currently, the porosity measurement methods for shale reservoirs involve low-temperature N_2 and CO_2 adsorption -desorption, field emission scanning electron microscopy (FE-SEM), 3D high-resolution image reconstruction technology and the Gas Research Institute (GRI) porosity method. The low-temperature gas adsorption-desorption method measures the connected pores that range from 0.38 to 100 nm in width; the results, however, are smaller than

* Corresponding author. E-mail: cfwdqpi@163.com

actual pore volumes because isolated pore volumes are ignored (Tian Hua et al., 2012; Ran Bo et al., 2016; Chen et al., 2018). Via the FE-SEM method, the microstructures of shale pores and especially those of organopores are visualized (Passey et al., 2010; Zou Caineng et al., 2011; Javier et al., 2017; Liu Yi et al., 2017), though these images are limited to 2D sections and cannot be quantitatively performed. The GRI method measures grain and bulk densities of shale samples via He pycnometry and Hg immersion, respectively and then calculates total porosity value (Chalmers et al., 2012; Utpalendu et al., 2014). The results of the GRI method include inevitable errors owing to organic-rich shale absorption, inconsistent crushing and sample handling procedures, varying relative humidity in measurement environment and solvent extraction pre-treatments that can remove solid organic matter (Utpalendu et al., 2014). 3D high-resolution image reconstruction is used to characterize the microstructures and evaluate the porosity value of a microscale shale cube sample (Ambrose et al., 2010; Curtis et al., 2012). However, the higher resolutions correspond with the smaller sample sizes (Long et al., 2009). The size of the shale cube sample is 1–5 μm in 3D high-resolution image reconstruction (Milner et al., 2010). Owing to greater heterogeneity in shale reservoir, the smaller samples are less representative than larger samples (Slatt and O'Brien, 2011). Furthermore, these methods cannot quantitatively evaluate the volumes of organic and inorganic pores. The amounts of adsorbed and free shale gas are directly affected by organic, inorganic, and total porosity values that are present in a shale sample. In this study, the Lower Silurian Longmaxi Formation shale in southeast Chongqing was selected as a case study. A method is introduced for estimating organic, inorganic and total porosity values, which can be used to study the development of shale gas.

2 Geological Settings

Southeast Chongqing has an area of approximately 1.98 × 10^4 km^2 and is located to the southwest of the Hubei Province, to the north of the Guizhou Province, and west of the Hunan Province. It is located within the Yangtze tectonic plate and is located in the Wuling Drape Zone and the western Hunan–Hubei thrust belt. The Xuefengshan Uplift and Sichuan Basin are to the east and northwest of southeast Chongqing, respectively (Fig. 1). The residual strata of Paleozoic age date to the Cambrian, Ordovician and Silurian periods; the other layers are denuded or missing. The Lower Paleozoic marine shales mainly include the Lower Cambrian Niutitang Shale and the Lower Silurian Longmaxi Formation shale, which are

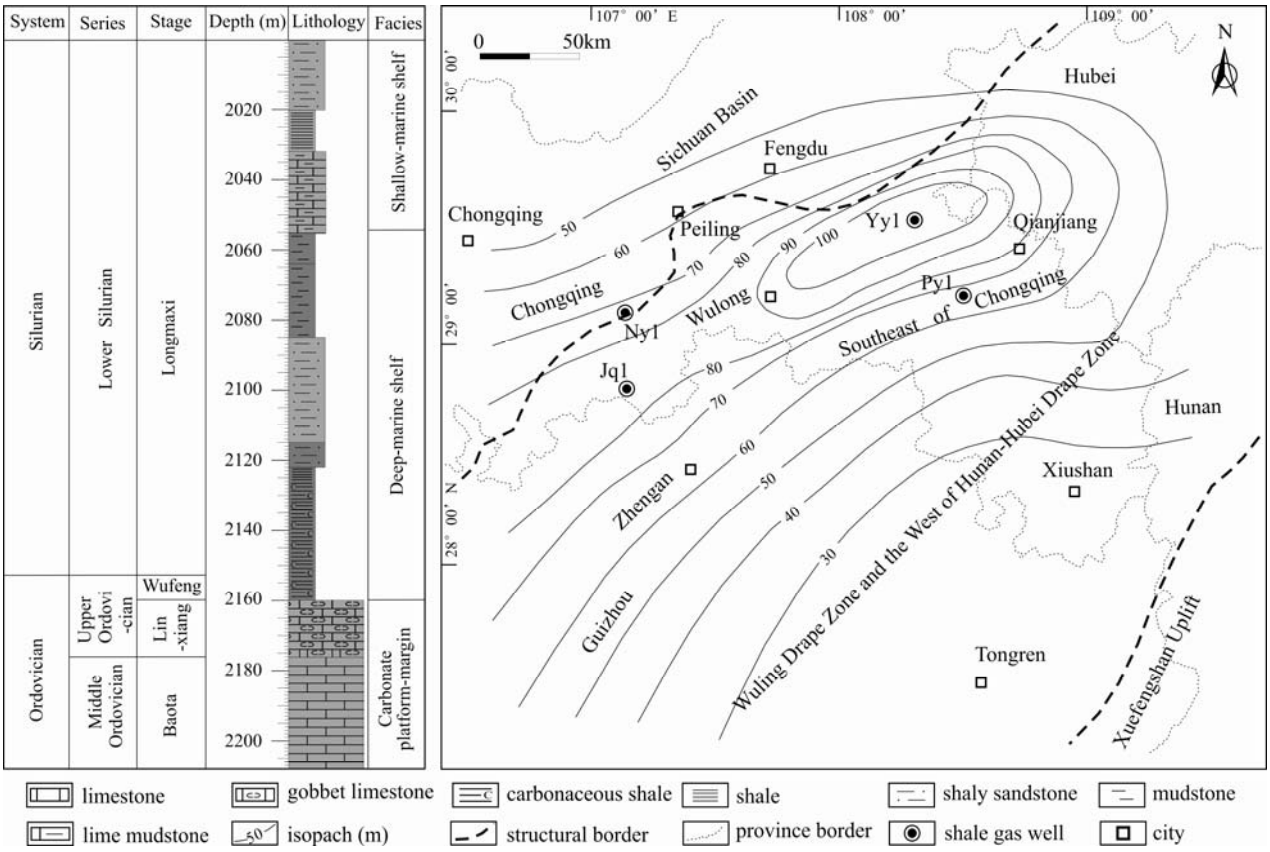

Fig. 1. Stratigraphic column and isopach map of the Longmaxi Formation shale in southeast Chongqing.

widely deposited in southeast Chongqing (Feng Dongjun et al., 2016; Liu Xiaoping et al., 2017). The Longmaxi Formation shale has yielded shale gas from all of the exploratory wells that have been drilled for shale gas exploration, such as Py1, Yy1, Jq1 and Ny1 (Fig. 1), and commercial gas flow has been obtained from several wells, including the Py1 well. These results indicate that the Longmaxi Formation shale in southeast Chongqing has a good exploration potential for shale gas.

3 Samples and Methods

Twenty-seven shale samples from cores from the Py1 well were selected for evaluating organic, inorganic, and total porosity values (Fig. 1). The geochemical characteristics and geological features of these samples, such as TOC, Rock-Eval parameters (S_0, S_1, S_2 and T_{max}), vitrinite reflectance (R_o), porosity from the GRI method, and mineral composition are shown in Table 1 and Table 2.

To identify and describe various pores in the shale samples, the FE-SEM method was employed. The bulk mass (M_B) was weighed using a balance set-up (Mettler Toledo AL104, readability 0.1 mg), and the bulk volume (V_B) was measured via mercury immersion at less than 6.6 Pa (50 μmHg) using Archimedes' Principle on a small chip of approximately 20 g without crushing after heating at 100°C for 12–16 h. The bulk density (ρ_B) was obtained dividing M_B by V_B. Given the high maturity of Longmaxi Formation shale (R_o>2.0%), type II_1-I organic matter and the absence of immature Longmaxi Formation shale in China, the Xiamaling Shale sample from the Huabei Platform was selected for pyrolysis testing. The Xiamaling Shale is similar to the source rocks of Longmaxi formation in southeast Chongqing but is less mature in comparison. The Xiamaling Shale is classified as type II_1 organic matter with a vitrinite reflectance (R_o) level of roughly 0.5% and with a TOC value of 5.98%.

4 Results

4.1 Various pores in organic-rich shale

4.1.1 Microfracture

Fractures of various widths and lengths in shale reservoir occur at a variety of scales, such as faults, joints and microfractures (Gale et al., 2007). Microfractures are microscopic reservoir spaces that can only be observed using SEM. In addition to tectonization, mineral crystallization also creates microfractures (Slatt and Abousleiman, 2011; Yuan Yuan et al., 2016; Wang Yuman et al., 2017). The microfractures in the Longmaxi Formation shale samples from Py1 well are usually less than 0.05 mm in width, and the majority of them extend across the viewing area of images (Figs. 2a and 2b). Compared with the artificial microfractures formed from well drilling and sample handling, precipitated calcite or deposited asphalt are often found in the natural microfractures.

4.1.2 Microchannel

The microchannels are corrugated discontinuous

Table 1 Geochemical characteristics of the Longmaxi Formation shale samples from the well Py1

Sample No.	Depth (m)	Vitrinite reflectance R_o (%)	Total organic carbon w (%)	Max temperature T_{max} (°C)	Gaseous hydrocarbon S_0 (mg/g)	Free hydrocarbon S_1 (mg/g)	Cracking hydrocarbon S_2 (mg/g)
1	2027.78	2.54	0.17	/	0.0003	0.0011	0.0004
2	2031.65	2.47	0.11	/	0.0001	0.0001	0.0038
3	2034.46	2.73	0.13	/	0.0009	0.0006	0.0042
4	2079.99	2.7	1.45	/	0.0013	0.0004	0.0035
5	2081.44	2.83	1.51	/	0.0006	0.0001	0.0034
6	2083.36	2.78	1.4	/	0.0013	0.0025	0.0094
7	2094.20	3.09	0.46	323.8	0.0019	0.0037	0.0104
8	2098.47	2.75	0.78	318.3	0.0028	0.0039	0.0115
9	2099.70	2.68	1.12	321.7	0.0028	0.0059	0.0091
10	2104.46	2.55	0.84	352.5	0.0100	0.0100	0.0200
11	2107.45	2.74	0.99	/	0.0021	0.0054	0.0077
12	2113.46	2.81	1.21	322.9	0.0024	0.0038	0.0111
13	2114.30	2.68	1.25	320.8	0.0022	0.0047	0.0068
14	2119.86	2.9	1.37	352.1	0.0027	0.0041	0.0119
15	2120.78	2.69	1.55	379.2	0.0023	0.0036	0.0081
16	2127.56	2.85	1.12	322.5	0.006	0.0087	0.0231
17	2128.49	2.91	1.21	320.8	0.0016	0.0039	0.0076
18	2132.61	2.66	1.66	332.1	0.0019	0.0044	0.0079
19	2133.95	2.79	1.51	/	0.0009	0.0001	0.0013
20	2138.13	2.76	2.38	/	0.0018	0.0017	0.0012
21	2141.89	2.74	2.59	320.8	0.0026	0.0059	0.0111
22	2146.13	2.81	3.32	345.4	0.0024	0.0042	0.0067
23	2149.60	2.68	3.9	320.8	0.0047	0.0087	0.0179
24	2150.84	2.87	3.81	/	0.0015	0.0001	0.0044
25	2156.55	2.77	4.12	/	0.0040	0.0085	0.0238
26	2157.76	2.79	2.52	/	0.0016	0.0007	0.0004
27	2158.28	2.89	0.27	365.4	0.0033	0.0067	0.0133

Note: The symbol "/" represents without data.

Table 2 GRI porosity values and mineralogical compositions of the Longmaxi Formation shale samples from Py1 well

Sample No.	Depth (m)	GRI porosity Φ (%)	Mineral compositions of shale rock (wt%)									Relative clay mineral content (wt%)			
			Quartz	Orthoclase	Plagioclase	Calcite	Dolomite	Aragonite	Pyrite	Barite	Clay	Illite	Chlorite	I/S	%S
1	2027.78	3.76	21.2	1.2	6.2	18.6	3.1	5.3	0.5	4.7	39.10	49	17	34	5
2	2031.65	3.13	23.1	1.1	5.4	22.6	4.9	4.7	1.6	3.9	32.63	36	18	46	5
3	2034.46	3.09	25.3	1.5	5.6	21.7	7.7	0.0	2.6	4.4	31.12	39	20	41	5
4	2079.99	4.16	29.8	1.6	8.3	3.1	0.0	4.8	3.8	3.9	44.70	38	15	47	5
5	2081.44	4.53	26.0	2.1	4.8	3.1	3.7	3.0	5.2	3.4	48.73	45	13	42	5
6	2083.36	3.10	27.0	1.8	6.7	2.6	5.4	0.0	4.8	4.5	47.26	35	16	49	5
7	2094.20	3.52	39.7	2.1	17.3	3.8	10.7	5.2	3.4	2.7	15.01	50	11	39	5
8	2098.47	3.87	36.8	4.5	12.4	5.8	6.8	4.6	2.9	4.6	21.49	40	10	50	5
9	2099.70	4.24	32.7	3.7	12.3	6.6	5.3	0.0	4.1	3.7	31.53	47	5	48	10
10	2104.46	3.50	30.5	3.2	12.3	5.1	5.6	0.0	4.2	4.2	34.75	48	12	40	5
11	2107.45	2.14	32.2	3.6	12.1	6.5	4.5	0.0	4.3	2.4	34.25	34	14	52	5
12	2113.46	2.82	33.6	4.2	10.8	5.3	6.3	3.7	3.2	5.2	27.73	39	11	50	5
13	2114.30	4.92	37.6	4.8	12.8	3.8	4.3	0.0	5.3	2.5	29.01	45	15	40	10
14	2119.86	3.92	33.0	3.4	11.2	6.0	2.8	0.0	5.7	3.1	34.81	40	10	50	10
15	2120.78	3.97	35.4	3.4	10.1	4.5	2.0	0.0	4.9	4.0	35.80	48	14	38	10
16	2127.56	4.56	36.7	3.9	12.2	3.8	1.9	0.0	4.1	5.8	31.43	40	13	47	10
17	2128.49	2.53	39.7	6.7	10.6	3.4	4.6	0.0	4.8	2.3	27.93	47	12	41	10
18	2132.61	3.90	33.8	3.6	11.9	5.4	2.5	0.0	3.9	1.7	37.26	44	13	43	10
19	2133.95	3.95	37.8	4.6	10.7	4.2	3.5	0.0	3.8	3.5	32.18	50	11	39	15
20	2138.13	4.68	39.2	4.1	6.8	9.1	4.8	4.9	6.7	3.3	21.12	56	7	37	5
21	2141.89	5.12	41.4	3.7	6.0	6.4	5.9	0.0	6.9	3.5	26.39	59	9	32	10
22	2146.13	6.75	43.3	2.8	5.8	6.1	5.8	2.7	6.8	5.7	20.98	43	14	43	5
23	2149.60	2.93	42.5	2.9	6.8	5.0	2.2	0.0	7.0	5.1	28.62	65	9	26	10
24	2150.84	4.84	41.1	3.1	6.9	4.7	7.5	0.0	7.5	7.1	22.24	45	8	47	10
25	2156.55	4.01	31.6	1.6	9.1	2.4	4.6	0.0	5.7	3.8	41.28	35	14	51	5
26	2157.76	2.86	32.2	3.2	10.1	0.0	6.8	0.0	4.3	3.8	39.68	36	7	57	5
27	2158.28	1.90	30.3	2.6	8.4	1.1	4.1	0.0	3.1	2.4	47.96	46	8	46	10

Note: I/S is the weight percentage of illite–smectite mixed-layer in clay minerals. %S represents the weight percentage of smectite in the illite–smectite mixed-layer.

microscopic channels in the shale matrix, which are nearly parallel with microlayer surfaces. Each microchannel is generally smaller than 0.3 μm in width with a length that does not transect the viewing area of image (Figs. 2c and 2d). The microchannels are not artefacts related to pressure release when a core is obtained from a drilling well. They are instead original microchannels that have survived within a shale matrix. Origins of microchannels include (1) residual microstructures of biological disturbance and (2) remnant microerosion surfaces of laminaes and microripples (Slatt and O'Brien, 2011).

4.1.3 Clay intergranular pore

Clay floccules usually form a “cardhouse” structure of individual edge-face- or edge-edge-oriented flakes and/or domains of face-face-oriented flakes (Fig. 2e) (Slatt and O'Brien, 2011; Lin Wen, 2016). Clay intergranular pores are common within this structure. These pores still exist in deeply buried ancient shale reservoir. How they have survived burial and diagenesis for hundreds of millions of years remains unknown (Slatt and O'Brien, 2011). These pores are much larger than methane molecules (0.38 nm) in width and provide permeability pathways for shale gas.

4.1.4 Intercrystalline pore within mineral aggregate

Intercrystalline pores exist within mineral aggregates or framboids. Pyrite framboids mixed with organic matter are common in the Longmaxi Formation shale (Figs. 2c, 2d, and 2f). There are intercrystalline pores within pyrite framboids, which comprise numerous pyrite crystals (Fig. 1f). The pyrite framboids usually occur in a dispersed pattern throughout the shale matrix. At the same time, the connectivity between the intercrystalline pores and the other types of pores is relatively poor. Their contributions to the porosity and permeability of the shale reservoir are relatively limited.

4.1.5 Intracrystalline pore

Intracrystalline pores derive from crystalline imperfection and dissolution within single crystalline mineral particles. These pores are isolated, infrequent, and not connected with other types of pores in shale matrix (Fig. 2g). Their contributions to the porosity and permeability of shale reservoir are very limited.

4.1.6 Organopore

Organopores are largely nanopores within organic matter grains, which formed from hydrocarbon generation during the process of thermal evolution (Curtis et al., 2010; Liu Shugen et al., 2011; Chalmers et al., 2012). Many scholars who have conducted research on organic porosity considered that the contributions of organopores to porosity values of shale samples are less than 3% (Christopher and Scott, 2012; Curtis et al., 2012). The FE-SEM images of the Lower Silurian Longmaxi Formation shale sample from Py1 well show that organopores are

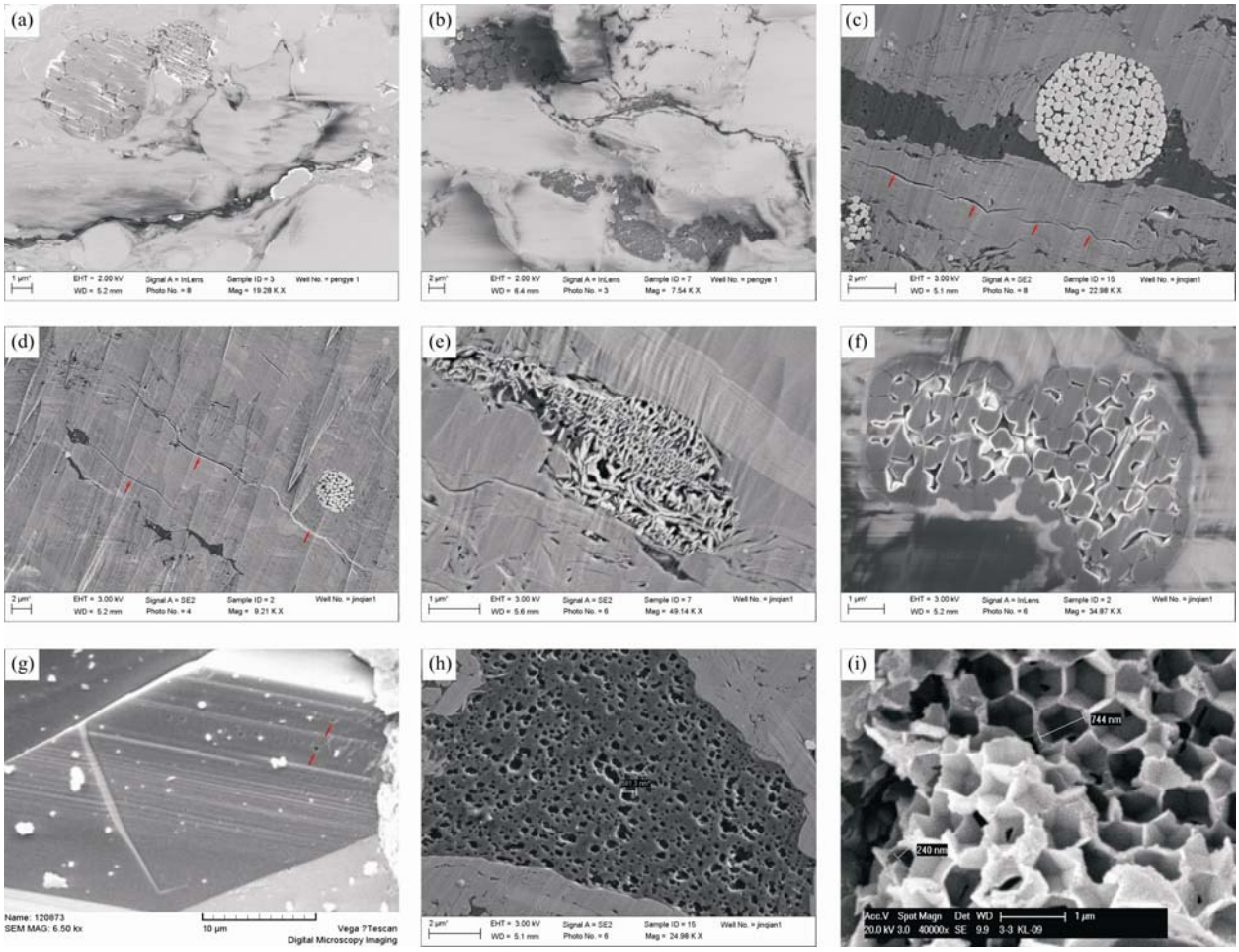

Fig. 2. The characteristics of nanoscale to microscale pores in the Longmaxi Formation shale samples from the well Py1 well southeast Chongqing.
(a) and (b), Microfractures; (c) and (d), Microchannels; (e), Interparticle pores containing clay flakes; (f), Intercrystalline pores within mineral grains; (g), Intracrystalline pore; (h), Organopores; (i), Fossil pores.

developed, and the connectivity of these organopores are good within a single organic matter grain (Fig. 2h). However, organic matter grains are generally dispersedly distributed in the Longmaxi Formation shale matrix. The overall connectivity of the organopores in the shale sample is low. Because of the lipophilicity and large specific surface area, organopores play a key role in the enrichment of adsorbed shale gas.

4.1.7 Fossil pore

Fossil pores are residual biological skeleton pores that are not filled with minerals or asphalts in biological fossils. In the Lower Silurian Longmaxi Formation shale of southeast Chongqing the biological fossils include diatom fossils (Fig. 2i) and graptolite fossils (Ma et al., 2016; Luo et al., 2016). Fossil pores are common in the Longmaxi Formation shale reservoir. There are some fossil pores as well as the organopores within organic matter grains (Ma et al., 2016; Luo et al., 2016), which play a significant role in the storage of shale gas. The fossil pores within organic matter grains, and the organopores were considered as organic pores to be evaluated in the following discussion.

4.2 Pyrolysis experiments

Pyrolysis experiments were performed from 200°C to 600°C under different heating rates using a Rock-Eval-II type pyrolysis instrument (30°C/h and 40°C/h). The hydrocarbon productions at corresponding temperatures (or times) were recorded. Then, the transformation ratios of hydrocarbon generated from organic matter (including the transformation ratios of oil and gas generated from kerogen) were obtained at different temperatures. These data were used to calibrate the chemical kinetics parameters (Fig. 3). Additional publications can be consulted for a description of the calibration method (Lu Shuangfang, 1996; Lu shuangfang et al., 2001; Wang et al., 2011).

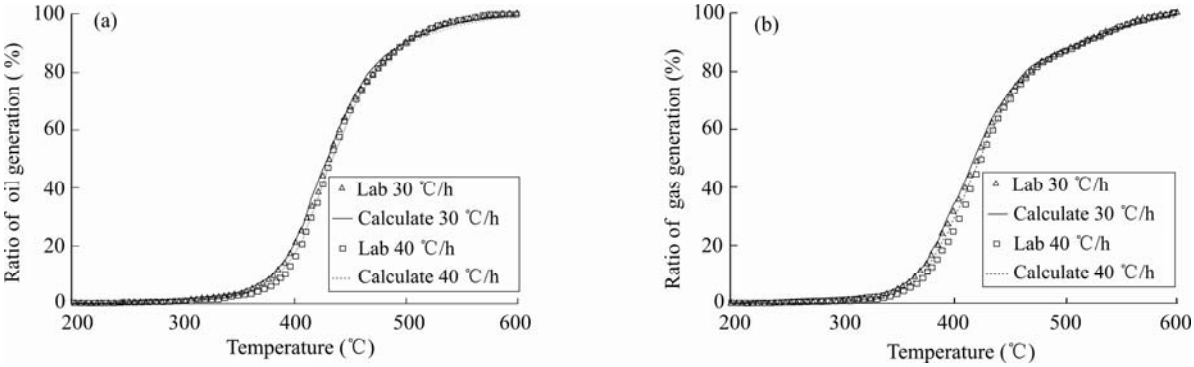

Fig. 3. Transformation ratio of oil and gas generated from organic matter at different temperatures and heating rates.
(a), Transformation ratio of oil generated from Xiamaling Shale kerogen; (b), Transformation ratio of gas generated from Xiamaling Shale kerogen.

5 Discussions

In examining microscopic pore contributions to pore space in shale samples, microscopic pores were divided into two categories: organic and inorganic pores. First, following the principle of material balance, the organic porosity values largely attributable to hydrocarbon generation were calculated. Second, these values were corrected using the organic porosity correction coefficient. The total porosity values were then calculated using the grain and bulk density values of the shale samples. Finally, the inorganic porosity values were calculated as the differences between the organic porosity values and the total porosity values.

5.1 Organic porosity of organic-rich shale

5.1.1 Model for evaluating organic porosity

According to the principle of material balance, under ideal conditions, the total volume of organic pores is equivalent to the volume of organic matter consumed through the hydrocarbon generating process (Formula 1) (Christopher and Scott, 2012; Chen et al., 2014). However, under actual geological conditions, compaction and liquid hydrocarbon bituminization processes are present. In addition, the fossil pores in the organic matter grains, such as graptolite pores (Luo et al., 2016), are not considered in the formulation of the material balance principle. Therefore, to more accurately simulate natural processes, organic porosity values calculated under ideal conditions should be corrected. A model was formulated to correct organic porosity values in shale samples as follows (Formula 2) (Chen et al., 2014):

$$\Phi_{\text{organic}} = w(\text{TOC}_0) \cdot I_{H0} \cdot F(R_o) \cdot \frac{\rho_{\text{rock}}}{\rho_{\text{kerogen}}} / 1000 \quad (1)$$

$$\Phi_{\text{organic-c}} = w(\text{TOC}_0) \cdot I_{H0} \cdot F(R_o) \cdot \frac{\rho_{\text{rock}}}{\rho_{\text{kerogen}}} / 1000 \cdot C \quad (2)$$

Following are the parameters in Formula 1 and Formula 2: Φ_{organic} is the organic porosity of a shale sample under ideal conditions (%); $\Phi_{\text{organic-c}}$ is the organic porosity of a shale sample in actual geological conditions (%); $w(\text{TOC}_0)$ is the weighted percentage of original total organic carbon (%); I_{H0} is the original cracking hydrocarbon of unit quality organic carbon (mg/g); $F(R_o)$ is the transformation ratio of oil and gas generated from kerogen (%), excluding the transformation ratio of gas generated from crude oil cracking; ρ_{rock} is the density of a shale sample (g/cm^3); ρ_{kerogen} is the density of kerogen, which is approximately 1.2 g/cm^3 (Okiongbo et al, 2005; Christopher and Scott, 2012) and C is the organic porosity correction coefficient.

The model includes four important parameters, namely the original total organic carbon [$w(\text{TOC}_0)$], the original hydrogen index (I_{H0}), the transformation ratio of oil and gas generated from kerogen [$F(R_o)$] and the organic porosity correction coefficient (C).

5.1.2 Transformation ratio of generated hydrocarbon

Combining with the burial and thermal history, the relationship between the transformation ratio of hydrocarbon generated from kerogen and elapsed geological time was determined using the results of pyrolysis experiments (Lu Shuangfang, 1996). The transformation ratios of oil and gas generated from kerogen in the Lonmaxi Shale are 67.9% and 27.5%, respectively.

5.1.3 Original hydrogen index and original total organic carbon

Following the restoration method of the original hydrogen index and original TOC, while combining the transformation ratio of hydrocarbon generated from kerogen, the original hydrogen index values and original TOC contents of the Longmaxi Formation shale samples

from Py1 well were restored according to Formula 3 and Formula 4 (Lu Shuangfang, 1996; Chen et al., 2014; Chen Fangwen et al., 2016). The original and residual hydrogen index values of the Longmaxi Formation shale samples from Py1 well range from 417.11–452.97 mg/g and 0.02–4.93 mg/g, with average values of 428.54 mg/g and 1.06 mg/g, respectively. The ranges of original and residual TOC contents are 0.31–10.64% and 0.11–4.12% with average values of 4.02% and 1.58%, respectively (Fig. 4).

$$I_{H0} = I_H + (I_{H0} \cdot F_o + B_0 - B) + I_{H0} \cdot F_g \quad (3)$$

$$w(\mathrm{TOC}_0) = w(\mathrm{TOC}) \cdot (1 + (I_{H0} - I_H) \cdot K / 1000) \quad (4)$$

Following are the parameters in Formula 3 and Formula 4: I_{H0} is the original hydrogen index (mg/g); I_H is the residual hydrogen index (mg/g); F_o is the transformation ratio of oil generated from kerogen (%); B_o is the native asphalt content (non-thermally decomposed from kerogen, mg); B is the residue oil content calculated from chloroform "A" or the hydrocarbon index by light/heavy hydrocarbon compensation (mg); F_g is the transformation ratio of gas generated from kerogen (%); w(TOC) is the weight percentage of the residual total organic carbon (%) and K is the coefficient of organic matter conversion into organic carbon, which is approximately 0.85 (Christopher and Scott, 2012).

5.1.4 Organic porosity correction coefficient

The organic porosity correction coefficient is the ratio of the actual organic porosity to the organic porosity formed through hydrocarbon generation under ideal conditions without compaction and liquid hydrocarbon bituminization. Within the same shale layer of a similar buried depth, because the differences of temperature and pressure conditions are marginal, processes of hydrocarbon generation, expulsion and diagenesis are nearly homogeneous. In turn, organic porosity correction coefficients are identical. To obtain the organic porosity correction coefficient, the FE-SEM method was applied to the shale samples from the same depth. The average surface porosity of organic pores was obtained via analysing the area ratios of organic pores to organic matter grains based on a set of FE-SEM images from the same depth. Surface porosity of organic pores ($\Phi_{SP\text{-}organic}$) was determined using area ratio of organic pores to organic matter grains, TOC, kerogen density and bulk density of shale sample (Formula 5). In turn, the organic porosity correction coefficient was calculated from the ratio of surface porosity of organic pores ($\Phi_{SP\text{-}organic}$) to organic

$$\Phi_{SP\text{-}organic} = A_{organic} \cdot w(\mathrm{TOC}) \cdot \frac{\rho_{rock}}{\rho_{kerogen}} \times 100\% \quad (5)$$

$$C = \Phi_{SP\text{-}organic} / \Phi_{organic} \quad (6)$$

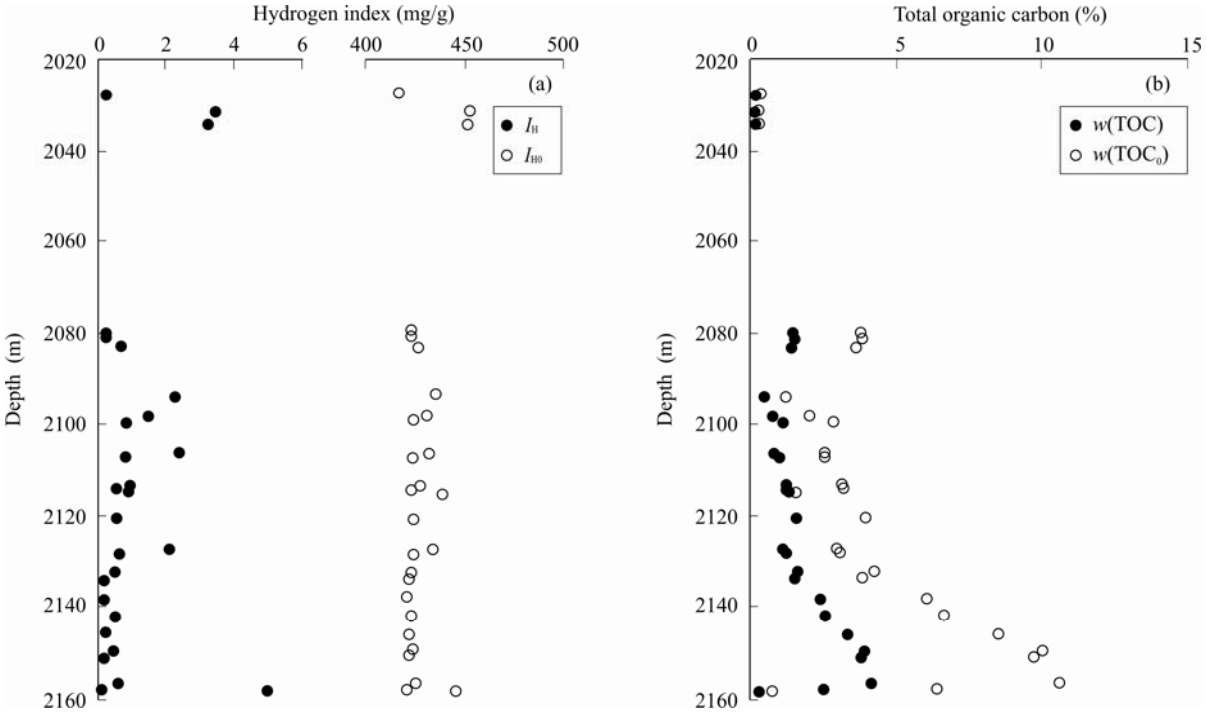

Fig. 4. Hydrogen index and total organic carbon values of the Longmaxi Formation shale samples from the well Py1 in southeast Chongqing.
(a), Hydrogen index; (b), Total organic carbon.

porosity ($\Phi_{organic}$) under ideal conditions (Formula 6).

In Formula 5 and Formula 6, $\Phi_{SP\text{-}organic}$ is the surface porosity of organic pores in shale sample (%), and $A_{organic}$ is the area ratio of organic pores to organic matter grains in FE-SEM images.

The sample No. 4 (see Tables 1 and 2) was selected to determine the area ratio of organic pores to organic matter grains by using the FE-SEM method (Figs. 5a, 5c, 5e and 5g). The sample No. 4 is 2079.99 m in depth with a TOC value of 1.45%. With increasing FE-SEM imaging magnification, the image resolutions have increased, and the smaller organic pores can be identified. However, the

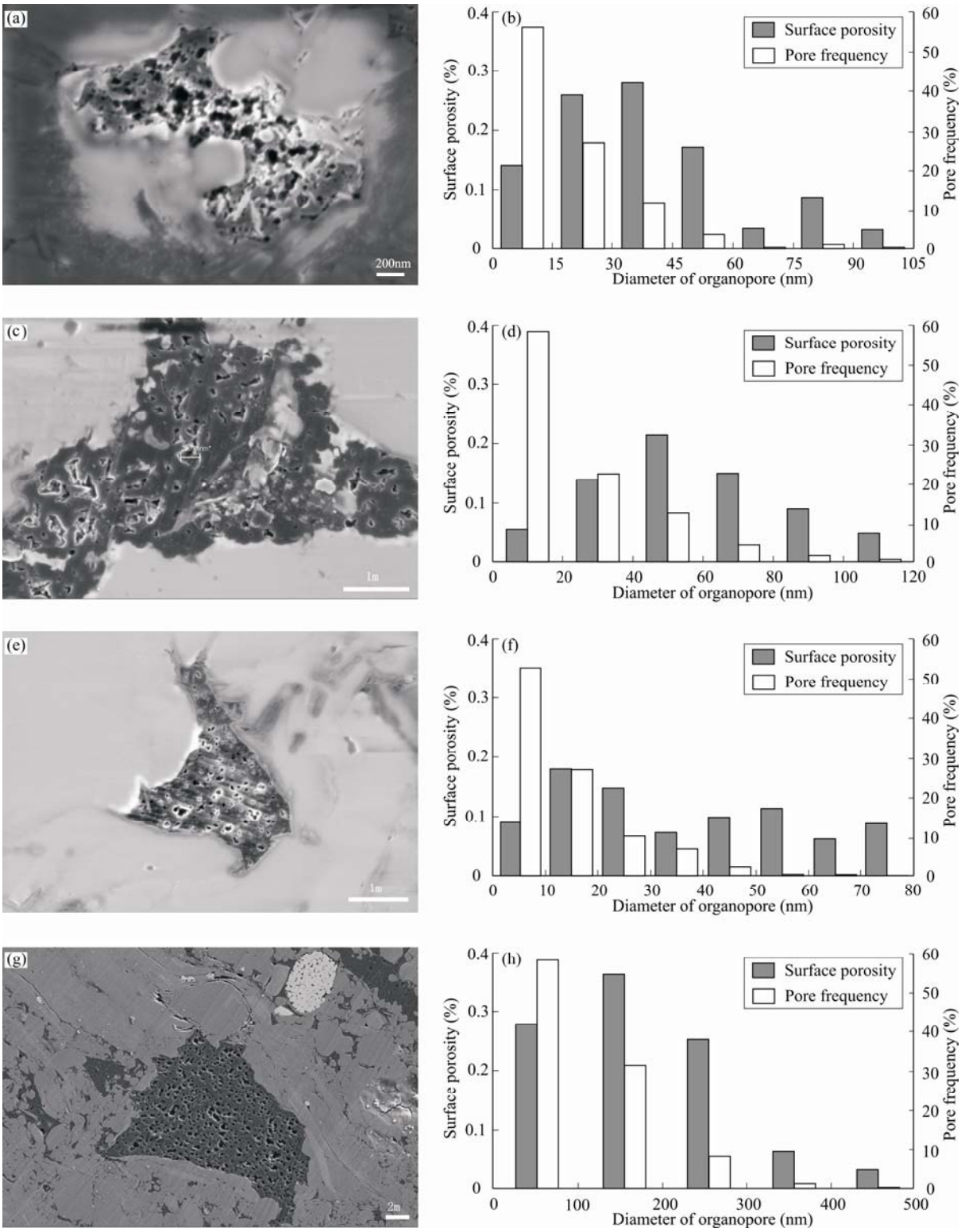

Fig. 5. The surface porosity values and frequencies of organic pores for sample No. 4 using FE-SEM method.

organic pores smaller than the FE-SEM resolution could not be identified. In this study, based on the frequencies of organic pores with different sizes that are identifiable, the frequencies of organic pores smaller than the resolution were fitted. Their areas were calculated using the area formula of a circle. Then, the area ratios of organic pores to organic matter grains in FE-SEM images were obtained. The surface porosity values of organic pores in the four FE-SEM images from sample No. 4 are 0.99%, 0.71%, 0.85% and 1.02% (Figs. 5b, 5d, 5f and 5h), respectively, with an average value of 0.89% according to Formula 5. The organic porosity correction coefficient is 0.28 based on the average surface porosity of organic pores (0.89%) divided by the organic porosity value of 3.20% under ideal conditions ($\Phi_{organic}$) according to Formula 6.

5.1.5 Organic porosity of organic-rich shale

Based on the transformation ratio of hydrocarbon generated from kerogen, the original hydrogen index, the original TOC and the organic porosity correction coefficient, the organic porosity values of the Longmaxi Formation shale samples from Py1 well in southeast Chongqing were determined (Formula 2). The uncorrected organic porosity (under ideal conditions) values range from 0.28%–9.00% with an average value of 3.40%. The corrected organic porosity values range from 0.08%–2.52% with an average value of 0.95%. The uncorrected and corrected organic porosity values of the Longmaxi Formation shale samples from Py1 well decreased gradually from the bottom to the top (Fig. 6).

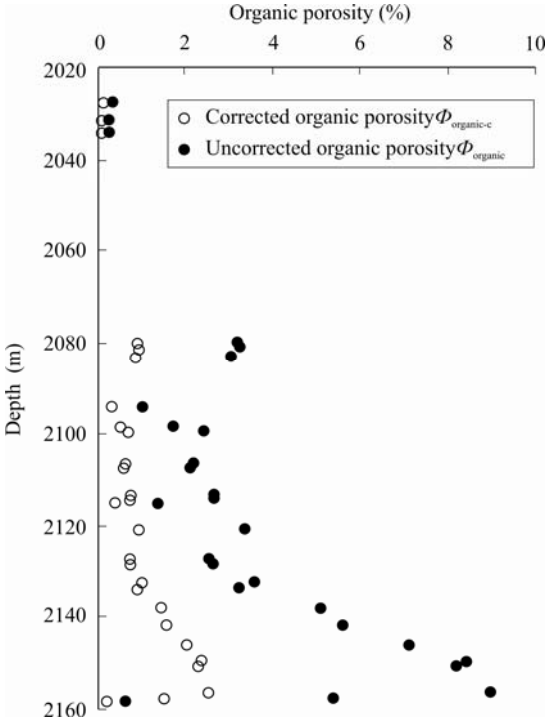

Fig. 6. Uncorrected and corrected organic porosity values of the Longmaxi Formation shale samples from the well Py1.

5.2 Total porosity of organic-rich shale

5.2.1 Model for evaluating total porosity

The total porosity (Φ_t) of organic-rich shale refers to the ratio of total pore volume to shale sample volume. It was calculated using the grain density (ρ_G) and bulk density (ρ_B) of the shale sample, as shown in Formula 7. The bulk density (ρ_B) of the sample is the ratio of the bulk mass (M_B) to the bulk volume (V_B). The grain density (ρ_G) of the shale sample was calculated using Formula 8.

$$\Phi_t = \frac{\rho_G - \rho_B}{\rho_G} \times 100\% \quad (7)$$

$$\rho_G = M / \left(\frac{m_1}{\rho_1} + \frac{m_2}{\rho_2} + \cdots + \frac{m_{n-1}}{\rho_{n-1}} + \frac{m_n}{\rho_n}\right) \quad (8)$$

In Formula 8, M is the unit mass of shale sample. m_1, m_2, …, m_{n-1} and m_n are the masses of various mineral and organic matter components in the unit mass of shale sample. ρ_1, ρ_2, …, ρ_{n-1} and ρ_n are the true density values of various components (Table 3), and n is the number of components in shale sample.

5.2.2 Total porosity of organic-rich shale

Following the total porosity evaluation model, the total porosity values of the Longmaxi Formation shale samples from Py1 well in southeast Chongqing were obtained by combining the contents of various components in the shale samples via X-ray diffraction and organic geochemical analysis. The total porosity values of these samples range from 2.75% to 6.14% with an average value of 4.34% (Fig. 7). The total porosity values and GRI porosity values of the 27 shale samples are very similar (Fig. 8). The differences between the results of the two methods range from 0.06% to 2.57% with an average value of 0.49%.

5.3 Inorganic porosity of organic-rich shale

The inorganic porosity is the ratio of inorganic pore

Table 3 True density values of various components (Pan Zhaolu, 1994; Okiongbo et al., 2005)

Density	Quartz	Orthoclase	Plagioclase	Calcite	Dolomite	Aragonite	Pyrite	Barite	Smectite	Chlorite	Illite	Organic matter
Max true density(g/cm^3)	2.65	2.57	2.76	2.80	3.20	3.00	5.20	4.60	2.70	3.60	2.90	1.20
Min true density(g/cm^3)	2.22	2.54	2.61	2.60	2.86	2.90	4.90	4.00	2.00	3.60	2.60	1.20
Average true density(g/cm^3)	2.44	2.56	2.69	2.70	3.03	2.95	5.05	4.30	2.35	3.60	2.75	1.20

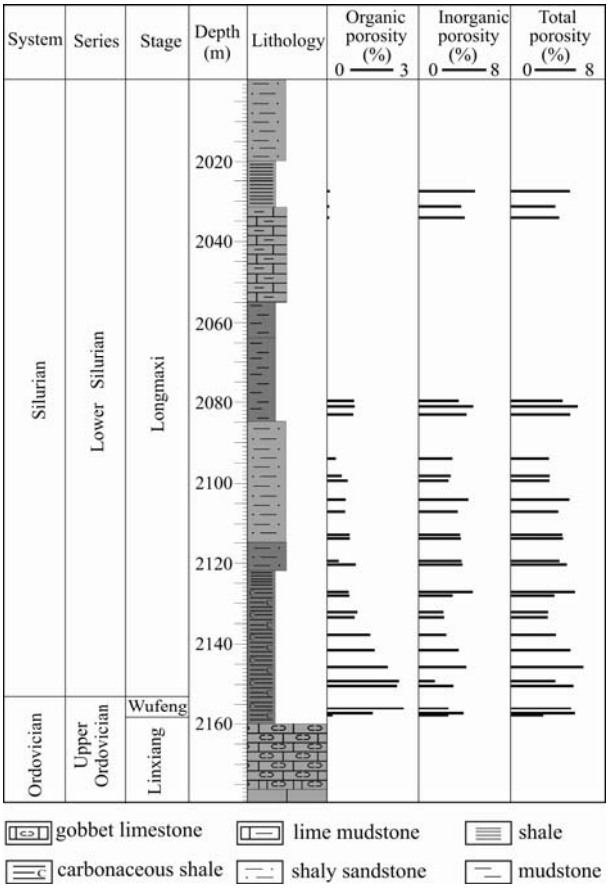

Fig. 7. Organic, inorganic and total porosity values of the Longmaxi Formation shale samples from the well Py1.

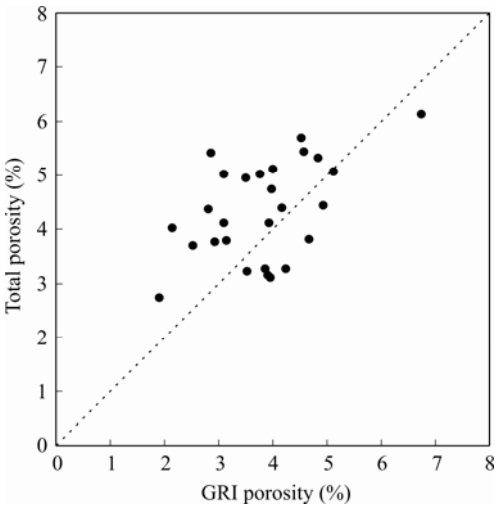

Fig. 8. Comparison of the total porosity values and the GRI porosity values of the Longmaxi Formation shale samples from the well Py1.
Note: The 1:1 comparison line is shown as a dotted line in the plot.

volume to the sample bulk volume, which is also the difference between the organic porosity and the total porosity. The inorganic porosity values of the Longmaxi Formation shale samples from Py1 well range from 1.41% to 4.92% with an average value of 3.39% (Fig. 7).

6 Conclusions

(1) In Longmaxi Formation shale of southeast Chongqing, the common microscale to nanoscale pores were divided into organic and inorganic pores. Inorganic pores primarily include microfractures, microchannels, clay intergranular pores, intercrystalline pores and intracrystalline pores. Organic pores primarily contain organopore within organic matter and fossil pore.

(2) For organic-rich shale samples, total porosity values are determined from the grain and bulk densities. Organic porosity values are calculated and corrected based on the chemical kinetics method and the organic porosity correction coefficient, respectively, and inorganic porosity values are the differences between the organic porosity and the total porosity values.

(3) The total, organic, and inorganic porosity values of the Longmaxi Formation shale samples from Py1 well range from 2.75%–6.14%, 0.08%–2.52% and 1.41%–4.92% with average values of 4.34%, 0.95% and 3.39%, respectively. The contributions of the inorganic pores to the total porosity are significantly greater than those of the organic pores in the Longmaxi Formation shale.

Acknowledgments

Financial supports from the National Science Foundation of China (grants No. 41530315, 41302101 and 41330313), the National Science and Technology Major Project of China (grant No. 2016ZX05061), the Natural Science Foundation of Shandong Province (grant No. ZR2016DL07) and the Fundamental Research Funds for the Central Universities (grant No. 18CX02071A) are acknowledged.

Manuscript received June. 11, 2017
accepted Aug. 10, 2017
edited by Hao Qingqing

References

Ambrose, R.J., Hartman, R.C., Diaz-Campos, M., Akkutlu, Y., and Sondergeld, C.H., 2010. New pore-scale considerations for shale gas in place calculations. In: *SPE Unconventional Gas Confertuobeience*, Society of Petroleum Engineers, 131772.

Chalmers, G.R.L., Bustin, R.M., and Power, I.M., 2012. Characterization of gas shale pore systems by porosimetry, pycnometry, surface area, and field emission scanning electron microscopy/transmission electron microscopy image analyses: examples from the Barnett, Woodford, Haynesville, Marcellus, and Doig units. *AAPG Bulletin*, 96(6): 1099–1119.

Chen, F.W., Lu, S.F., and Ding, X., 2014. Organoporosity evaluation of shale: a case study of the Lower Silurian Longmaxi Shale in southeast Chongqing, China. *The*

Scientific World Journal, 893520.

Chen, F.W., Lu, S.F., Ding, X., He, X.P., and Xing, H.L., 2018. The splicing of backscattered scanning electron microscopy method used on evaluation of microscopic pore characteristics in shale sample and compared with results from other methods. *Journal of Petroleum Science and Engineering*, 160 (1): 207–218.

Chen, F.W., Lu, S.F., Ding, X., He, X.P., and Xing, H.L., 2017. Evaluation of the Adsorbed Gas Amount in a Shale Reservoir Using the Three Compositions Adsorbing Methane (TCAM) Method: A Case from the Longmaxi Shale in southeast Chongqing, China. *Energy & Fuels*, 31(1): 11523–11531.

Chen Fangwen, Lu Shuangfang and Ding Xue, 2016. Gas generation period and quantity of organic-rich Niutitang Shale in Qiannan Depression, China. Journal of China University of Petroleum, 40(3): 55–62 (in Chinese with English abstract).

Chen Lei, Jiang Zhenxue, Liu Keyu, Gao Fenglin and Wang Pengfei, 2017. A combination of N_2 and CO_2 adsorption to characterize nanopore structure of organic-rich Lower Silurian shale in the Upper Yangtze Platform, South China: implications for shale gas sorption capacity. *Acta Geologica Sinica* (English Edition), 91(4): 1380–1394.

Christopher, J.M., and Scott, G.L., 2012. Estimation of kerogen porosity in source rocks as a function of thermal transformation: example from the Mowry Shale in the Powder River Basin of Wyoming. *AAPG Bulletin*, 96(1): 87–108.

Curtis, M.E., Ambrose, R.J., Sondergeld, C.H., and Rai, C.S., 2010. Structural characterization of gas shales on the micro- and nano-scales. In: *Canadian Unconventional Resources and International Petroleum Conference*, Society of Petroleum Engineers, 137693.

Curtis, M.E., Sondergeld, C.H., Ambrose, R.J., and Rai, C.S., 2012. Microstructural investigation of gas shales in two and three dimensions using nanometer-scale resolution imaging. *AAPG Bulletin*, 96(4): 665–677.

Gale, J.F.W., Reed, R.M., and Holder, J., 2007. Natural fractures in the Barnett Shale and their importance for hydraulic fracture treatments. *AAPG Bulletin*, 91(4): 603–622.

Feng Dongjun, Hu Zongquan, Gao Bo, Peng Yongmin and Du Wei, 2016. Analysis of shale gas reservoir—forming condition of Wufeng Formation—Longmaxi Formation in Southeast Sichuan Basin. *Geological Review*, 62(6): 1521–1532 (in Chinese with English abstract).

Han Shuangbiao, Zhang Jinchuan, Yang Chao, Lin Lamei, Zhu Liangliang, Chen Yongchang and Xue Bing, 2013. The characteristics of nanoscale pore and its gas storage capability in the Lower Cambrian shale of southeast Chongqing. *Journal of China Coal Society*, 38(6): 1038–1043 (in Chinese with English abstract).

Howard, J.J., 1991. Porosimetry measurement of shale fabric and its relationship to illite/smectite diagenesis. *Clays and Clay Minerals*, 39(4): 355–361.

Jarvie, D.M., Hill, R.J., Ruble, T.E., and Pollastro, R.M., 2007. Unconventional shale-gas systems: the Mississippian Barnett Shale of north-central Texas as one model. *AAPG Bulletin*, 91 (4): 475–499.

Javier, S.A.C., Boris, I.K., Thelma, E.S.Q., and Toma´s, C.H.G., 2017. Micro- and nanoporous materials capable of absorbing solvents and oils reversibly: the state of the art. *Petroleum Science*, 14(1): 84–104.

Lin Wen, 2016. A review on shale reservoirs as an unconventional play – the history, technology revolution, importance to oil and gas industry, and the development future. *Acta Geologica Sinica* (English Edition), 90(5): 1887-1902.

Liu Shugen, Ma Wenxin, Lubomir Jansa, Huang Wenming, Zeng Xianliang and Zhang Changjun, 2011. Characteristics of the shale gas reservoir rocks in the Lower Silurian Longmaxi formation, East Sichuan Basin, China. *Acta Petrologica Sinica*, 27(8): 2239–2252 (in Chinese with English abstract).

Long, H., Swennen, R., Foubert, A., Dierick, M., and Jacobs, P., 2009. 3D quantification of mineral components and porosity distribution in Westphalian C sandstone by microfocus X-ray computed tomography. *Sedimentary Geology*, 220: 116–125.

Loucks, R.G., Reed, R.M., Ruppel, S.C., and Jarvie, D.M., 2009. Morphology, genesis, and distribution of nanometer-scale pores in siliceous mudstones of the Mississippian Barnett shale. *Journal of Sedimentary Research*, 79(12): 848–861.

Lu Shuangfang, 1996. *Kinetics theory of hydrocarbon generation from organic matter and its application*. Beijing: Petroleum Industry Press, 136 (in Chinese).

Lu Shuangfang, Liu Xiaoyan, Fu Xiaotai, Feng Yali, Wang Zhenping and Xue Haitao, 2001. Chemical kientics study on the generation mechanism of immature to low-mature oil and its initial application. *Acta Sedimentologica Sinica*, 19(1): 130–135 (in Chinese with English abstract).

Luo, Q.Y., Zhong, N.N., Dai, N., Zhang, W., 2016. Graptolite-derived organic matter in the Wufeng–Longmaxi Formations (Upper Ordovician–Lower Silurian) of southeastern Chongqing, China: implications for gas shale evaluation. *International Journal of Coal Geology*, 153: 87–98.

Ma, Y., Zhong, N.N., Cheng, L.J., Pan, Z.J., Dai, N., Zhang, Y., Yang, L., 2016. Pore structure of the graptolite-derived OM in the Longmaxi Shale, southeastern Upper Yangtze Region, *China. Marine and Petroleum Geology*, 72: 1–11.

Milner, M., McLin, R., and Petriello, J., 2010. Imaging texture and porosity in mudstones and shales: Comparison of secondary and ion-milled backscatter SEM methods. In: *Canadian Unconventional Resources and International Petroleum Conference*, Society of Petroleum Engineers, 138975.

Mosher, K., He, J.J., Liu, Y.Y., Rupp, E., and Wilcox, J., 2013. Molecular simulation of methane adsorption in micro- and mesoporous carbons with applications to coal and gas shale systems. *International Journal of Coal Geology*, 109–110: 36–44.

Okiongbo, K.S., Aplin, A.C., and Larter, S.R., 2005. Changes in type II kerogen density as a function of maturity: Evidence from the Kimmeridge Clay formation. *Energy Fuels*, 19(6): 2495–2499.

Pan Zhaolu, 1984. *Crystallography and Mineralogy* (2nd edition). Beijing: Geological Publishing House, 274 (in Chinese).

Passey, Q.R., Bohacs, K.M., Esch, W.L., Klimentidis, R., and Sinha, S., 2010. From oil-prone source rock to gas-producing shale reservoir: geologic and petrophysical characterization of unconventional shale-gas reservoirs. In: *International Oil and Gas Conference and Exhibition in China*, Society of Petroleum Engineers, 131350.

Ran Bo, Liu Shugen, Luba Jansa, Sun Wei, Yang Di, Wang Shiyu, Ye Yuehao, Christopher Xiao, Zhanhg Jian, Zhai Cangbo, Luo Chao and Zhang Changjun, 2016. Reservoir

characteristics and preservation conditions of Longmaxi shale in the Upper Yangtze Block, South China. *Acta Geologica Sinica* (English Edition), 90(6): 2182–2205.

Slatt, R.M., and Abousleiman, Y., 2011. Merging sequence stratigraphy and geomechanics for unconventional gas shales. *The Leading Edge*, 30(3): 274–282.

Slatt, R.M., and O'Brien, N.R., 2011. Pore types in the Barnett and Woodford gas shales: contribution to understanding gas storage and migration pathways in fine-grained rocks. *AAPG Bulletin*, 95(12): 2017–2030.

Tian Hua, Zhang Shuichang, Liu Shaobo and Zhang Hong, 2012. Deterination of organic-rich shale pore features by mercury injection and gas adsorption methods. *Acta Petrolei Sinica*, 33 (3): 419–427 (in Chinese with English abstract).

Utpalendu, K., Douglas, K.M., Arkadiusz, D., Timothy, B.F., and Manika, P., 2014. Total porosity measurement in gas shales by the water immersion porosimetry (WIP) method. *Fuel*, 117: 1115–1129.

Wang, M., Lu, S.F., and Xue, H.T., 2011. Kinetic simulation of hydrocarbon generation from lacustrine type I kerogen from the Songliao Basin: model comparison and geological application. *Marine and Petroleum Geology*, 28, 1714–1725.

Wang Yuman, Wang Hongkun, Zhang Chenchen, Li Xinjing and Dong Dazhong, 2017. Fracture pore evaluation of the Upper Ordovician Wufeng to Lower Silurian Longmaxi Formations in southern Sichuan Basin, SW China. *Petroleum Exploration and Development*, 44(4): 563–572.

Wei Xiangfeng, Zhao Zhengbao, Wang Qingbo, Liu Zhujiang, Zhou Min and Zhang Hui, 2017. Comprehensive evaluation on geological conditions of the shale gas in Upper Ordovician Wufeng Formation—Lower Silurian Longmaxi Formation in Dingshan area, Qijiang, Southeastern Sichuan. *Geological Review*, 63(1): 153–164 (in Chinese with English abstract).

Xiao Xianming, Wei Qiang, Gai Haifeng, Li Tengfei, Wang Maolin, Pan Lei, Chen Ji and Tian Hui, 2015. Main controlling factors and enrichment area evaluation of shale gas of the Lower Paleozoic marine strata in south China. *Petroleum Science*, 12: 573–586.

Yuan Yuan, Jiang Zhenxue, Yu Chen, Wang Pengfei, Guo Tianxu, Zhao Ruotong and Tang Xianglu, 2016. Reservoir characteristics of high abundance and low thermal stage lacustrine shale: An example from the Middle Jurassic shale in the Northern Qaidam Basin. *Acta Geologica Sinica*, 90(3): 541–552 (in Chinese with English abstract).

Zhao Jianhua, Jin Zhijun, Jin Zhenkui, Wen Xin and Geng Yikai, 2016. Physical mechanism of organic matter-mineral interaction in Longmaxi Shale, Sichuan Basin, China. *Acta Geologica Sinica* (English Edition), 90(5): 1923–1924.

Zhao Wenzhi, Li Jianzhong, Yang Tao, Wang Shufang and Huang Jinliang, 2016. Geological difference and its significance of marine shale gases in South China. *Petroleum Exploration and Development*, 43(4): 547–559.

Zou Caineng, Zhu Rukai, Bai Bin, Yang Zhi, Wu Songtao, Su Ling, Dong Dazhong and Li Xinjing, 2011. First discovery of nano-pore throat in oil and gas reservoir in China and its scientific value. *Acta Petrologica Sinica*, 27(6): 1857–1864 (in Chinese with English abstract).

About the first author

CHEN Fangwen, born in Hubei in 1984, received his doctoral degree from Northeast Petroleum University and is now a lecturer at Research Institute of Unconventional Oil & Gas and Renewable Energy, China University of Petroleum (East China). His main research interests include the characteristics of shale gas reservoirs and resource evaluation. Address: No. 66, Changjiang W Rd, Huangdao District, Qingdao, 266580.E-mail: chenfw@upc.edu.cn.